Journal of Materials Chemistry A

Understanding the effects of oxygen defects on the redox reaction pathways in $LiVPO_4F$ by combining *ab-initio* calculations with experiments

Journal:	*Journal of Materials Chemistry A*
Manuscript ID	TA-ART-03-2019-003070.R1
Article Type:	Paper
Date Submitted by the Author:	20-Apr-2019
Complete List of Authors:	Park, Heetaek; Pohang University of Science and Technology, Department of Materials Science and Engineering Kim, Minkyung; Pohang University of Science and Technology, Department of Materials Science and Engineering Kang, ShinYoung; Lawrence Livermore National Laboratory Kang, Byoungwoo; Pohang University of Science and Technology, Department of Materials Science and Engineering

ARTICLE

Understanding the effects of oxygen defects on the redox reaction pathways in $LiVPO_4F$ by combining *ab-initio* calculations with experiments

Received 00th January 20xx,
Accepted 00th January 20xx

DOI: 10.1039/x0xx00000x

Heetaek Park, [a] Minkyung Kim, [a] ShinYoung Kang, *[b] and Byoungwoo Kang *[a]

Tavorite $LiVPO_4F$ has a great potential as a cathode material due to its high energy density, superior thermal stability and fast kinetics. It has been controversial whether the redox reaction pathway of $LiVPO_4F$ is symmetric or not, but the origin of such symmetric/asymmetric redox reaction pathways has not been clearly understood. By combining *ab-initio* calculations with experiments, we found that oxygen defects on fluorine sites, O_F^-, can be a key factor that affects the symmetry of redox pathway of $LiVPO_4F_{1-\delta}O_\delta$ ($\delta < 1$). The computational results indicate that 1) the thermodynamically metastable 'triclinic' polymorph of $VPO_4F_{1-\delta}O_\delta$, which maintains the structural symmetry of the $LiVPO_4F$, can be kinetically stabilized considering its marginally higher energy than the stable 'monoclinic' phase; and 2) the O_F^- defects slightly destabilize the intermediate phase (x = 0.667) ($Li_{0.667}VPO_4F$ versus $Li_{0.667}VPO_4F_{0.917}O_{0.083}$), inferring that the presence of O_F^- defects can induce the asymmetric redox pathway of $LiVPO_4F_{1-\delta}O_\delta$. We also experimentally found that the concentration of O_F^- defects is critically affected by the synthesis process of $LiVPO_4F$, and VPO_4F with lower O_F^- concentration can support the possible presence of the metastable (triclinc) phase, leading to the redox pathway prone to be symmetric. Therefore, controlling oxygen defects by a synthesis processes can affect electrochemical performance via different redox reaction pathways of $LiVPO_4F$. This understanding provides further possibilities for improving the electrochemical performance.

1. Introduction

Because Performance of Li-ion batteries (LIBs), such as energy density, life time, safety, and power, highly depends on materials[1] Thus understanding material properties is required to move forward to high-performance LIB technology. Since the appearance of $LiCoO_2$, many interesting cathode materials have been suggested for many years.[2, 3] On the other hand, there are many electrode materials for LIBs that undergo the formation of intermediate phases during discharging and charging processes. One of the examples is a tavorite-type structure compound such as $LiVPO_4F$, $LiFeSO_4OH$, and $LiFeSO_4F$,[4-6] which have intermediate phases such as $Li_{0.67}VPO_4F$, $Li_{0.5}FeSO_4OH$ and $Li_{0.5}FeSO_4F$, respectively. An olivine $LiFePO_4$ compound has been of interest in academic and industrial fields because of its high performance in nanoparticles.[7] Despite the phase separation during charge/discharge, which was believed to degrade the kinetics of charge/discharge reactions due to nucleation and growth of a new phase in a phase separating compound,[8-10] the formation of metastable intermediate Li_xFePO_4 ($x < 1$) phase is only observed during high C-rate charging/discharging.[9, 11, 12] In addition, it has been confirmed that different phase transformation pathway in $LiFePO_4$ nanoparticles during charge/discharge can be a main reason for achieving high performance.[7, 10] Given that the battery performance is closely tied to the phase transformation mechanisms, mechanistic understanding of the phase transformation behavior in electrode materials, especially for phase separating materials, is essential for further improvement of battery performance.

Tavorite $LiVPO_4F$ is a promising cathode material due to its high energy density and fast kinetics.[13] Vanadium can have four oxidation states from 2+ to 5+, and tavorite $LiVPO_4F$ can take more than one mole of Li in its structure, enabling to achieve high energy density.[14] Using *in-situ* X-ray diffraction (XRD), Mba *et al.* found that $LiVPO_4F$ synthesized by Carbon Thermal Reduction (CTR) process underwent two biphasic processes, from $LiVPO_4F$ to $Li_{0.67}VPO_4F$ and then to VPO_4F only during the charge, whereas it followed a two-phase reaction from VPO_4F directly to $LiVPO_4F$ in the discharge, even at the same C-rate (Figure 1a).[4] On the other hand, Piao *et al.* observed a little different phase transformation pathway through *in-situ* X-ray absorption near-edge spectroscopy (XANES) for $LiVPO_4F$, which was also synthesized by the CTR process (Figure 1b).[15] A symmetric phase transformation pathway ($LiVPO_4F \leftrightarrow Li_xVPO_4F \leftrightarrow VPO_4F$) was observed, and the lithium content in the intermediate phase ranges from x =

[a] Department of Materials Science and Engineering, Pohang University of Science and Technology (POSTECH), 77 Cheongamro, Namgu, Pohang, Gyeongbuk, Republic of Korea 790-784
[b] Lawrence Livermore National Laboratory, Livermore, California 94550, USA

† Electronic Supplementary Information (ESI) available: [Conversion procedures of unit cell of $LiVPO_4F$, and results of NEB calculations]. See DOI: 10.1039/x0xx00000x

(a) **Redox pathway 1 (ref. 4)**

Charge: $LiVPO_4F \rightarrow Li_{0.67}VPO_4F \rightarrow VPO_4F$

Discharge: $VPO_4F \rightarrow LiVPO_4F$

(b) **Redox pathway 2 (ref. 15)**

Charge: $LiVPO_4F \rightarrow Li_xVPO_4F \rightarrow VPO_4F$

Discharge: $VPO_4F \rightarrow Li_xVPO_4F \rightarrow LiVPO_4F$

where x = 0.25~0.80

Figure 1. (a) Asymmetric and (b) symmetric redox pathways of $LiVPO_4F$ proposed in the previous studies.

0.25 to 0.80, not a fixed value at x = 0.67. Furthermore, a $LiVPO_4F$ prepared with a new synthesis process using polytetrafluoroethlene, $(-CF_2-CF_2-)_n$, (PTFE process) instead of the conventional carbon thermal reaction (CTR) process exhibits the asymmetric phase transformation pathway similar to Mba *et al.,* but much higher rate capability up to 20C could be achieved.[14] Understanding of the origin of this discrepancy in the redox reaction pathways demands more systematic studies depending on the synthesis and testing conditions.

Bamine *et al.* recently reported that oxygen defects in fluorine sites, O_F^- can be existed in $LiVPO_4F$ synthesized by the CTR process.[16] The paper reported that the fluorine supply was not sufficient during the synthesis process, and thereby the amount of the unintended and uncontrolled oxygen defects could be involved when $LiVPO_4F$ was synthesized by the CTR process. However, in the PTFE process, sufficient fluorine can be provided from additional PTFE,[14] and thus the concentration of O_F^- may be possibly reduced. To understand the synthesis-dependent battery performance and the effect of O_F^- on the phase transformation pathway, we investigated the role of O_F^- to the redox mechanism of $LiVPO_4F$ by density functional theory (DFT) calculations combined with experiments. Firstly, structure and composition-dependent stability of Li_xVPO_4F and $Li_xVPO_4F_{0.917}O_{0.083}$ ($0 \le x \le 1$) were calculated to understand the correlation between O_F^- and the symmetry of redox pathway. Also, our experiments found that the synthesis method, i.e. CTR and PTFE, can determine the amount of the O_F^- based on the lattice parameters and dihedral angles between VO_4F_2 octahedra. By combining DFT calculations with experimental observations, we conclude that the combinatorial impacts of the stability of the intermediate phases ($Li_{0.667}VPO_4F$ and $Li_{0.667}VPO_4F_{0.917}O_{0.083}$), phase transformation kinetics, and the stability of fully delithiated (VPO_4F and $VPO_4F_{0.917}O_{0.083}$) phases may affect the symmetry of redox reaction pathways depending on the existence of the O_F^-.

2. Method

2.1 Computational setting

Total energies of Li_xVPO_4F and $Li_xVPO_4F_{0.917}O_{0.083}$ ($0 \le x \le 1$) were calculated using the Vienna ab initio simulation package (VASP)[17] with the projector-augmented wave (PAW) method.[18] We used the Perdew-Burke-Ernzerhof (PBE) generalized gradient approximation (GGA)[19] functional and on-site Hubbard U correction on vanadium of 3.1 eV[20] reported in Wang *et al*.[21] A 3×2×1 supercell containing 12 formula units along with a plane-wave energy cut-off of 520 eV and 2×3×5 *k*-points were used. The optimization was stopped until the energy converges within 10^{-6} eV/atom.

2.2 Computation of monoclinic and triclinic VPO_4F and energy barrier for their phase transition

2.2.1 Structural conversion from monoclinic VPO_4F to triclinic one

It is reported that the unit cell symmetry of Li_xVPO_4F increases upon delithiation: triclinic ($P\bar{1}$) for $LiVPO_4F$ and $Li_{0.67}VPO_4F$, and monoclinic (C2/c) for VPO_4F.[4] A structural difference between triclinic and monoclinic phases is whether the orientations of corner-shared VO_4F_2 octahedra are aligned (monoclinic) or tilted (triclinic). In experiments, only monoclinic VPO_4F is reported, but we created a hypothesized 'triclinic VPO_4F' phase by fully extracting Li ions from triclinic $LiVPO_4F$. The ground state structures of triclinic $LiVPO_4F$ and monoclinic VPO_4F are

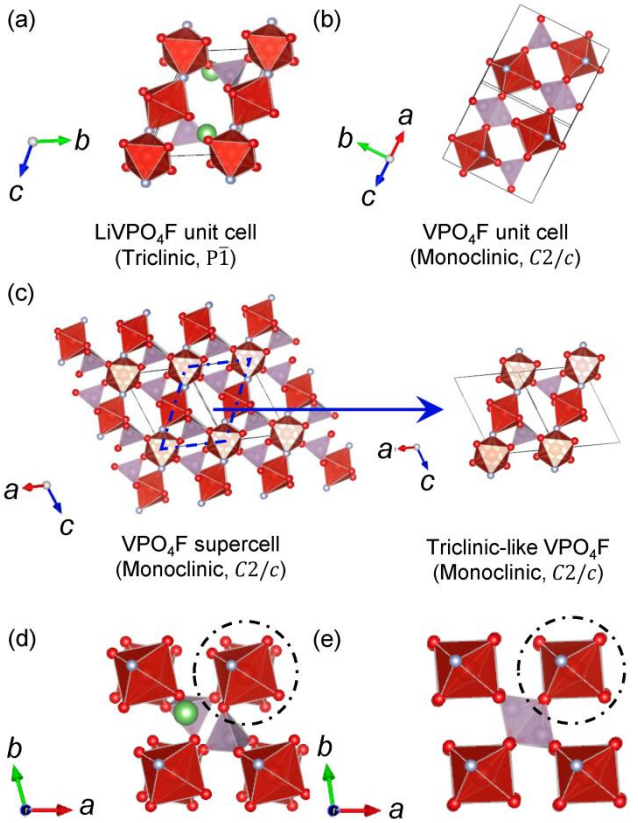

Figure 2. Illustration of the stable polymorphs of (a) $LiVPO_4F$ in the triclinic $P\bar{1}$ space group and (b) VPO_4F in the monoclinic C2/c space group. (c) The monoclinic VPO_4F supercell converted to "triclinic-like" lattice following the structural conversion processes explained in the text. The alignment of VO_4F_2 octahedra in (d) the triclinic $LiVPO_4F$ and (e) the triclinic-like VPO_4F converted from monoclinic structure along with the *c*-axis direction. The VO_4F_2 octahedron is highlighted with black dotted circles. Red octahedra and purple tetrahedra represent VO_4F_2 and PO_4, respectively, and green and red spheres represent lithium and oxygen, respectively.

displayed in Figures 2a and 2b. To directly compare triclinic VPO_4F (with tilted VO_4F_2 octahedra) to monoclinic VPO_4F (with aligned VO_4F_2 octahedra), we converted the unit cell of monoclinic VPO_4F to resemble lattice parameters of the triclinic phase (Figure 2c). Hereafter, we label this converted monolinic VPO_4F to a tricilinic one by "triclinic-like". Details for conversion procedures of monoclinic VPO_4F to a "triclinic-like" lattice is explained in Supplementary Information (SI). The alignments of VO_4F_2 octahedra can be clearly compared between triclinic $LiVPO_4F$ and "triclinic-like" VPO_4F in Figures 2d and 2e.

2.2.2 Energy barrier for the phase transition between monoclinic and triclinic $VPO_4F_{1-\delta}O_\delta$

As aforementioned, triclinic ($P\bar{1}$) and monoclinic (C2/c) $Li_xVPO_4F_{1-\delta}O_\delta$ phases have almost identical structures, except the alignment of VO_4F_2 octahedra. It is worth noting that the VO_4F_2 tilting distortion, in other words the presence of metastable triclinic $VPO_4F_{1-\delta}O_\delta$, has not taken attention in most previous studies.[22-24] However, the dihedral angle between VO_4F_2 can be served as a characteristic of triclinic and monoclinic phases; the dihedral angle ≈ 0 for the monoclinic phase and the dihedral angle > 0 for the triclinic, helping the identification of these phases in experiments. Moreover, this phenomenon can play an important role in the formation of intermediate phases and thus the phase transformation pathways. The correlation between tilting angles and subsequent phase transformation pathways will be discussed in detail in following sessions.

To figure out the correlation between the dihedral angle and energetics of the delithiated phases (VPO_4F and $VPO_4F_{0.917}O_{0.083}$), the activation energy for phase transition from triclinic and monoclinic $VPO4F_{1-\delta}O_\delta$ (δ = 0 and 0.083) was calculated using the climbing-image solid-state nudged elastic band (CI-SSNEB) method.[25-30] A 3×2×1 supercell and six intermediate images were employed. Lattice parameters (*a, b, c, α, β, γ*) and VO_4F_2 dihedral angles were investigated at each image fully-optimized within CI-SSNEB.

2.3 Calculations of the total energies of Li_xVPO_4F and $Li_xVPO_4F_{0.917}O_{0.083}$ ($0 \le x \le 1$)

The overall computations were performed using the triclinic lattices as hinted from experiments for $LiVPO_4F$ and $Li_{0.67}VPO_4F$.[4] The ground state energies of Li_xVPO_4F with x = 0.917, 0.833, 0.667, 0.500, 0.333, 0.167, and 0.083 were calculated by optimizing cell shape, volume, and ionic positions. For x = 0.917, 0.833, 0.167, and 0.083, all possible Li/vacancy distributions over Li sites were considered. For x = 0.667, 0.500, and 0.333, due to exhaustive number of possible partial occupancies, we chose 48, 64, and 48 distributions considering the symmetry and electrostatics, respectively. The Gibbs free energies (ΔG) were calculated by adding configurational entropies (ΔS_{conf}) at 25 ºC. The configurational entropies of the phases were computed as $\Delta S_{conf}(x) = -k_B \cdot [x \cdot \ln x + (1-x) \cdot \ln(1-x)]$, where x is mole franction of Li in $Li_xVPO_4F_{1-\delta}O_\delta$ and k_B is Bolzmann constant, considering that the Li sites in triclinic $LiVPO_4F$ are all equivalent.[13, 14]

Similarly, total energies of $Li_xVPO_4F_{0.917}O_{0.083}$ ($0 \le x \le 1$) with O_F^- were also calculated using the lowest energy Li/vacancy configuration of Li_xVPO_4F. Also, in order to confirm feasibility of the oxygen defect formation, the defect formation energy (ΔE_{form}) was calculated as follows (eq. 1):

$$\Delta E_{form} = E(LiVPO_4F_{0.917}O_{0.083}) - E(LiVPO_4F) + E(F_2)/24 - E(O_2)/24 \quad (1)$$

2.4 Experimental processes for investigation of $LiVPO_4F$.

$LiVPO_4F$ sample were prepared by two synthesis processes: 1) PTFE process and 2) Carbon thermal reduction (CTR) process.[4, 14]

1) PTFE process: LiF, V_2O_5, $NH_4H_2PO_4$, polytetrafluoroethylene (PTFE) 25 wt% and stearic acid ($C_{18}H_{36}O_2$) 5% of total weight of other precursors (LiF, V_2O_5, $NH_4H_2PO_4$) were ball-milled in acetone for 12 hours and then dried. Stearic acid was used for formation carbon coating layer on $LiVPO_4F$ particles. The mix of the precursors was pressed into a solid pellet, annealed at 700 °C for 1 hr under Ar and then naturally cooled down to room temperature.

2) Carbon thermal reduction (CTR) process: V_2O_5, $NH_4H_2PO_4$ and carbon (C) were ball-milled in acetone for 1 day and then dried (V_2O_5 : $NH_4H_2PO_4$: C = 0.5 : 1 : 1 mol ratio). The mix of the precursors was pelletized and then annealed at 900 °C for 4h under Ar. VPO_4/C phase was synthesized firstly. After first annealing, VPO_4/C and LiF was mixed well and then annealed at 700 °C for 1h under Ar and then quenched from 700 °C to room temperature.

Delithiated phases of PTFE and CTR samples were also prepared by electrochemical delithialtion process. Electrochemical cells of $LiVPO_4F$ obtained by PTFE and CTR processes were prepared as we introduced in the previous study.[14] The electrodes were rinsed with diethyl carbonate (DEC) in an Ar-filled glovebox and dried after charging the electrochemical cells up to 4.5 V. Synchrotron X-ray diffraction patterns on the $LiVPO_4F$ powder samples and VPO_4F electrodes were collected using beamline 9B at Pohang accelerator laboratory (PAL) in Korea. Fixed theta is 7°, and the data collected every 0.02° for 4s. Reitveld refinement of VPO_4F was carried out by using X'pert Highscore Plus software. The structure information was obtained from B.L.Ellis *et al.*'s.[23]

3. Results

3.1 Stability of the delithiated phases and transformation energy barrier between monoclinic and triclinic $VPO_4F_{1-\delta}O_\delta$

3.1.1 Structural difference between monoclinic and triclinic VPO_4F

In experiments, $LiVPO_4F$ and VPO_4F were found in the triclinic and monoclinic phases, respectively.[4, 24] Before investigating the stability of Li_xVPO_4F (0 < x < 1) intermediates, the ground states of triclinic and monoclinic VPO_4F ($VPO_4F_{0.917}O_{0.083}$) were calculated. It should be noted again that the "triclinic-like"

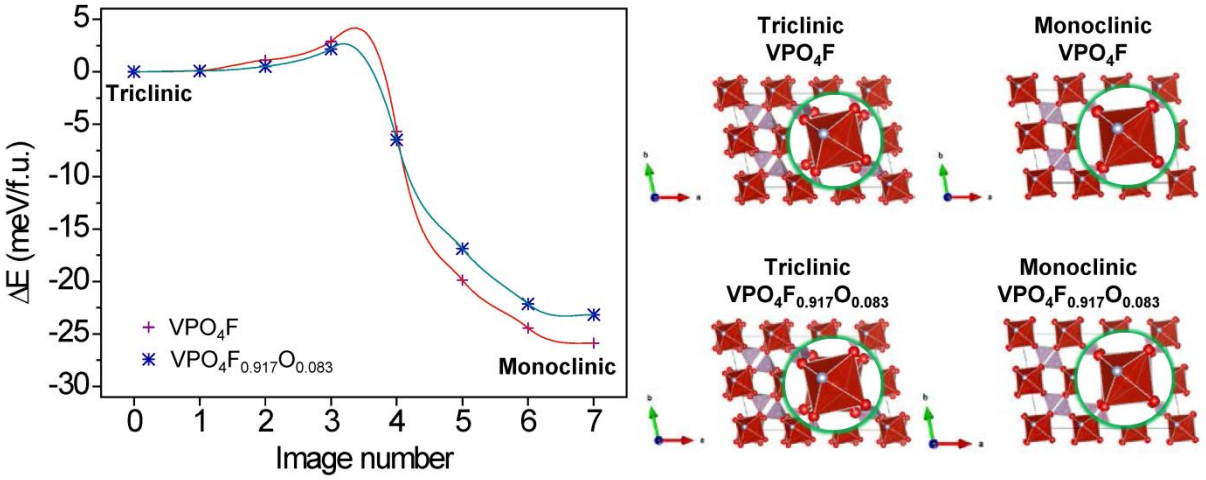

Figure 1. (a) Phase transition energies for triclinic ↔ monoclinic VPO_4F and $VPO_4F_{0.917}O_{0.083}$ computed in SSNEB calculations and (b) illustrated local structures of triclinic and monoclinic VPO_4F ($VPO_4F_{0.917}O_{0.083}$). One of the VO_4F_2 octahedron units are enlarged in green circles for clearly visualizing their orientational alignments (different tilting angles). The formation energy is referenced to that of the triclinic phases.

Table 1. Calculated energy barriers (E_a) from triclinic to monoclinic VPO_4F and $VPO_4F_{0.917}O_{0.083}$ and vice versa.

E_a (meV/f.u.)	Triclinic → Monoclinic	Monoclinic → Triclinic
VPO_4F	4	30
$VPO_4F_{0.917}O_{0.083}$	3	26

monoclinic VPO_4F ($VPO_4F_{0.917}O_{0.083}$) was obtained by converting the ground state monoclinic VPO_4F ($VPO_4F_{0.917}O_{0.083}$) to a triclinic lattice for directly comparing with "triclinic" VPO_4F ($VPO_4F_{0.917}O_{0.083}$) (see SI for details).

3.1.2 Different phase transition of the delithiated phases such as triclinic and monoclinic VPO_4F depending on the existence of oxygen defects

In our calculations, the monoclinic structure is a thermodynamically stable phase irrespective of the presence of the oxygen defects because the triclinic phase is higher in energy by 26 (for VPO_4F) and 23 meV (for $VPO_4F_{0.917}O_{0.083}$) per formula unit (meV/f.u.) than the monoclinic phase. This is consistent with the experimental observation. Therefore, it is evident that the equilibrium reaction pathway lets the triclinic $LiVPO_4F_{1-\delta}O_\delta$ undergo a phase transition to monoclinic $VPO_4F_{1-\delta}O_\delta$ at the end of charging. The calculated activation energies for the phase transition from the triclinic VPO_4F ($VPO_4F_{0.917}O_{0.083}$) to the monoclinic VPO_4F ($VPO_4F_{0.917}O_{0.083}$) obtained from climbing-image solid-state nudged elastic band (CI-SSNEB) are 4 meV/f.u for VPO_4F and 3 meV/f.u. for $VPO_4F_{0.917}O_{0.083}$ (Figure 3 and Table 1). This indicates that the phase transformation is almost barrier-less and the remaining triclinic $VPO_4F_{1-\delta}O_\delta$ structure can only exist as metastable in experiments regardless of the presence of the oxygen defects. However, this metastability of the triclinic $VPO_4F_{1-\delta}O_\delta$ can differ the stability of intermediate phases, $Li_xVPO_4F_{1-\delta}O_\delta$ where $0 < x < 1$, with and without the oxygen defects and hence redox reaction behavior. The impact of the oxygen defects on the stability of the intermediate phases by that of the delithiated phases will be discussed in section 3.2.

3.1.3 Structural change during the phase transition of the delithiated phases from the monoclinic phase to the triclinic one

The phase transition from the triclinic to the monoclinic $VPO_4F_{1-\delta}O_\delta$ phase is accompanied with the rotation/distortion of VO_4F_2 octahedra and volume changes as shown in Figure 4. The evolution of lattice parameters and average dihedral angles of O2-V1-V2-O4 and O1-V1-V2-O3 sites ($\theta1$ and $\theta2$) is plotted as a function of transition coordinates in Figure S4 in SI and Figure 4, respectively. Regardless of the presence of O_F^-, the dihedral angle and volume of the triclinic phase are larger than those of the monoclinic phase. However, the dihedral angles in the triclinic and monoclinic structures without O_F^- (VPO_4F) are higher than those with O_F^- ($VPO_4F_{0.917}O_{0.083}$), indicating that the incorporation of O_F^- can relieve intrinsic mechanical strains and decrease dihedral angles of PO_4F_2

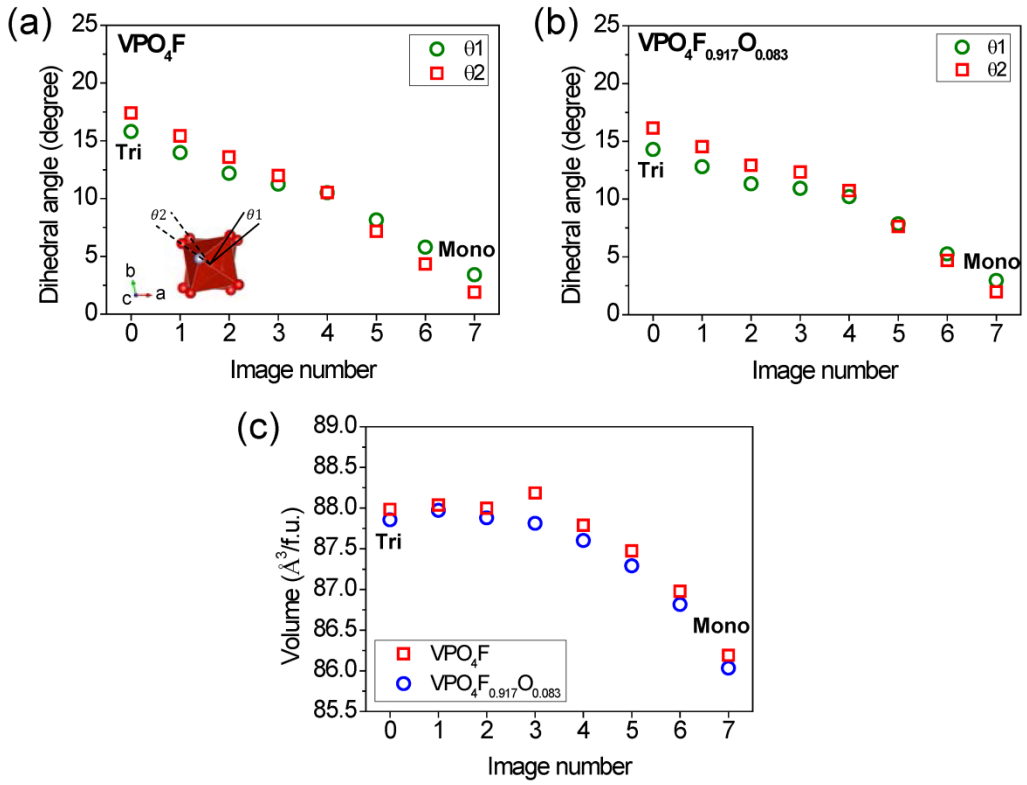

Figure 2. Evolution of dihedral angles of VO_4F_2 octahedra in a phase transition from the triclinic phase to the monoclinic phases in (a) VPO_4F and (b) $VPO_4F_{0.917}O_{0.083}$, and (c) volume changes of VPO_4F and $VPO_4F_{0.917}O_{0.083}$ using optimized structures within SSNEB calculations.

octahedra in $VPO_4F_{0.917}O_{0.083}$. Also, the dihedral angle of the delithiated phases monotonically decreases by transforming from the triclinic phase to the monoclinic one while the evolution of volume is bulged near to the energy maxima. As a result, the dihedral angle between VO_4F_2 octahedra can be utilized as an indicator for identifying the triclinic and monoclinic $VPO_4F_{1-\delta}O_\delta$ polymorphs.

3.2 Effects of oxygen defects (O_F^-) on the stability of the intermediate phases during charge/discharge process

Although the energy difference between $VPO_4F_{1-\delta}O_\delta$ phases with and without oxygen defect was not significant (Figure 3), the stability of the intermediate phases between $LiVPO_4F$ and the delithiated phases can be altered by the presence of O_F^-. Figure 5 shows the calculated formation energies of the intermediate phases (Li_xVPO_4F and $Li_xVPO_4F_{0.917}O_{0.083}$ where x = 0.083, 0.167, 0.333, 0.500, 0.667, 0.833, and 0.917) as a function of Li content. It should be noted that the energies of $Li_xVPO_4F_{0.917}O_{0.083}$ phases were calculated using the lowest formation energy of the Li/vacancy configurations predicted in defect-free Li_xVPO_4F. Figure 5a shows the energies of intermediate phases as a function of Li content with the reference to the energies of triclinic VPO_4F and $LiVPO_4F$ without O_F^-. The Li/vacancy arrangements in the intermediate phases were sampled using the "triclinic" structure. Combining with the configurational entropies, the Gibbs free energies ($\Delta G = \Delta E - T\Delta S_{conf}$) of Li_xVPO_4F and $Li_xVPO_4F_{0.917}O_{0.083}$ were calculated as explained in the Method section and plotted in Figure 5b.

After incorporating the configurational entropy term, it was confirmed that the stability of intermediate phases strongly depends on whether the delithiated phases ($VPO_4F_{1-\delta}O_\delta$) are stabilized in the triclinic or monoclinic structure as well as the presence of oxygen defect. First of all, the equilibrium pathway is between triclinic $LiVPO_4F_{1-\delta}O_\delta$ and monoclinic $VPO_4F_{1-\delta}O_\delta$ passing through intermediates at x = 0.667 and 0.833 for both with and without the oxygen defects (Path "2" in Figure 5). Except the fact that a few other intermediates at x = 0.333 and 0.5 are also < 3 meV above the $LiVPO_4F$-monoclinic VPO_4F tie line for defect free system, which can be accessible by thermal energies, there is no strike effect of oxygen defects on the equilibrium reaction pathway. However, when it comes to the non-equilibrium pathway connecting the triclinic $LiVPO_4F_{1-\delta}O_\delta$

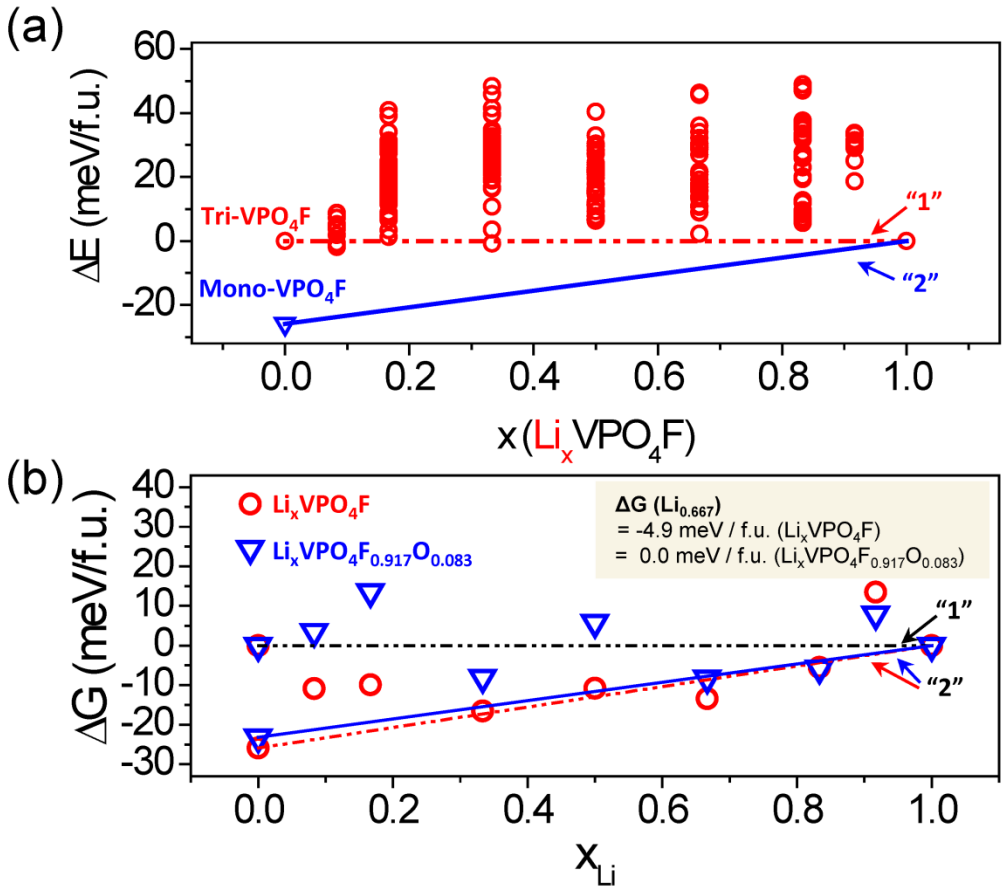

Figure 3. (a) Calculated energies of Li_xVPO_4F phases reference to the energies of triclinic VPO_4F and $LiVPO_4F$ and (b) calculated Gibbs free energies of Li_xVPO_4F and $Li_xVPO_4F_{0.917}O_{0.083}$ combined with configurational entropy ($-T\Delta S_{conf}$) at 25 ℃.

and metastable triclinic $VPO_4F_{1-\delta}O_\delta$ (Path "1" in Figure 5), the stability of intermediates substantially changes depending on the presence of oxygen defects: For defect-free Li_xVPO_4F system, most of intermediates are significantly stabilized (similar to redox reaction pathway 2 in Figure 1), whereas for the oxygen defective $Li_xVPO_4F_{0.917}O_{0.083}$ system only one more intermediate at x = 0.333 is stabilized (similar to redox reaction pathway 1 in Figure 1).

Taking a close look into the experimentally observed intermediate phases with x = 0.667 ($Li_{0.667}VPO_4F$ and $Li_{0.667}VPO_4F_{0.917}O_{0.083}$), their formation energies with respect to the tie line of triclinic $LiVPO_4F$ (or $LiVPO_4F_{0.917}O_{0.083}$) and stable monoclinic VPO_4F (or $VPO_4F_{0.917}O_{0.083}$) are -4.9 meV for $Li_{0.667}VPO_4F$ and 0.0 meV for $Li_{0.667}VPO_4F_{0.917}O_{0.083}$. This indicates that the incorporation of O_F^- strongly destabilizes the *x* = 0.667 intermediate phase. In other words, the $Li_{0.667}VPO_4F_{1-\delta}O_\delta$ intermediate phase during charge and discharge is more likely to form in defect-free $LiVPO_4F$, while its appearance highly depends on the state (triclinic or monoclinic) of the delithiated phase for the oxygen defective $LiVPO_4F_{0.917}O_{0.083}$.

3.3 Experimental observations

3.3.1 Formation of the oxygen defects on fluorine sites

Based on the DFT calculations, the incorporation of O_F^- causes different structural distortions such as different dihedral angle as shown in Figure 4. To verify the effects of O_F^- on the structure of the $LiVPO_4F$ in experiments, we prepared the $LiVPO_4F$ samples using two different synthesis processes: One process is the PTFE method that can provide fluorine-rich environment during a synthesis and the other is the CTR method that is reported to likely form O_F^- defects by providing limited fluorine environment during synthesis.[16] Figures 6a and 6b show the results of Rietveld refinement analysis of the $LiVPO_4F$ samples prepared by PTFE and CTR methods, respectively. Details of the XRD refinement of the materials

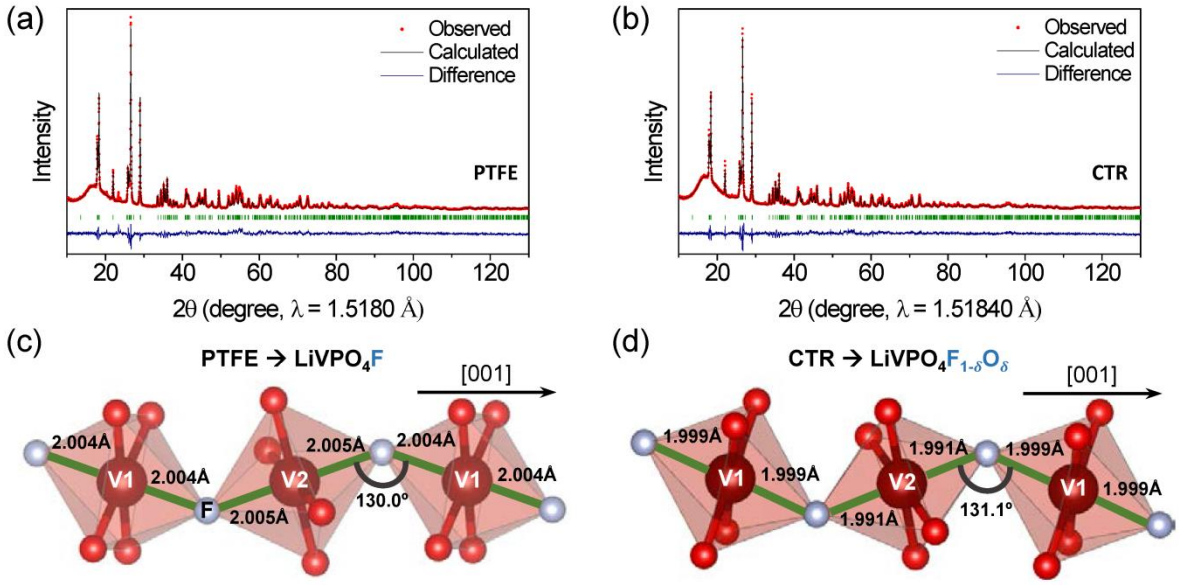

Figure 4. Rietveld refinement results of synchrotron XRD patterns of (a) the PTFE and (b) the CTR samples. Configuration of VO_4F_2 octahedron chains along the *c*-axis direction of (c) PTFE and (d) CTR samples

Table 2. Comparison of lattice parameters of $LiVPO_4F$ obtained by experiments (PTFE and CTR) and DFT calculations

	a (Å)	*b* (Å)	*c* (Å)	alpha (°)	beta (°)	gamma (°)	V/Z (Å^3)
PTFE	5.184	5.312	7.266	107.58	107.95	98.45	87.48
CTR, this study	5.176	5.308	7.265	107.58	107.98	98.36	87.31
$LiVPO_4F$ (DFT)	5.259	5.401	7.473	108.70	107.95	97.24	92.61
$LiVPO_4F_{0.917}O_{0.083}$ (DFT)	5.256	5.400	7.438	108.65	107.83	97.33	92.19

are included in Supplementary Information (Table S1 and S2). Bamine *et al.* reported that the CTR-$LiVPO_4F$ has dilute O_F^-,[16] and we also reported that vanadium in the CTR sample can have a higher oxidation state than that in the PTFE sample indicating the incorporation of the oxygen defect.[14] In $LiVPO_4F_{1-\delta}O_\delta$ ($0 \le \delta \le 1$) system, lattice parameters (*a*, *b*, *c*, and volume V) become smaller as the oxygen defect concentration, 'δ' increases. Also, the local structure of VO_4F_2 octahedra changes: the V-F bond lengths decrease and the angle of V-F-V between two corner-sharing VO_4F_2 octahedra increases as a result of oxygen incorporation.[13, 24] To figure out the possible effect of the sample preparation methods on the O_F^- concentration, the local structure (Figures 6c and 6d) and lattice parameters (Table 2) of the two samples were obtained from synchrotron XRD and then compared. The V-F bond lengths in the PTFE-$LiVPO_4F$ were 2.004 and 2.005 Å, which are longer than those in the CTR-$LiVPO_4F$, 1.999 and 1.991 Å. Lattice parameters were also differed by the preparation methods. The molar volume of the CTR sample in this study (V/Z = 87.31 Å^3) was 0.15 % smaller than that of the PTFE sample (V/Z = 87.48 Å^3). The molar volume and V-F bond lengths inform the higher O_F^- concentration in the CTR sample compared to the PTFE sample.

Also, lattice parameters of the samples were compared with those of $LiVPO_4F$ and $LiVPO_4F_{0.917}O_{0.083}$ calculated in DFT in Table 2. The calculated values were slightly overestimated compared to the corresponding experimental ones, in general, due to the well-known under-binding nature of the GGA functional.[31] Nevertheless, the molar volume of defect free $LiVPO_4F$ is 0.46 % larger than that of $LiVPO_4F_{0.917}O_{0.083}$, demonstrating that the oxygen defect concentration can depend on molar volume of $LiVPO_4F$. Considering that molar volume of the PTFE sample is higher than that of the CTR sample, the relative oxygen defect concentrations in the samples can be in the range between $LiVPO_4F$ and $LiVPO_4F_{0.917}O_{0.083}$. Note that the calculated formation energy of the oxygen defects (eq. 1) was 142.4 meV, which might be accessible during fluorine-deficient synthesis conditions, such

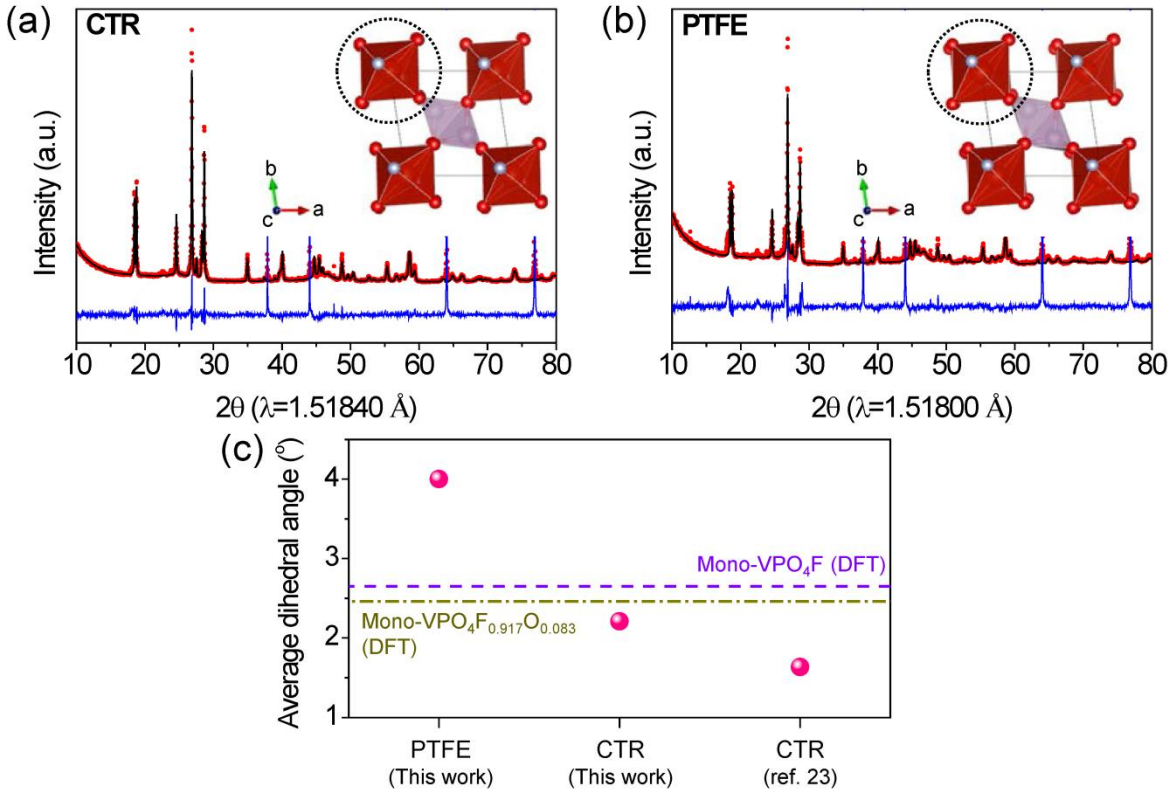

Figure 5. Synchrotron X-ray diffraction patterns of $VPO4F_{1-\delta}O_{\delta}$ phases obtained by electrochemically delithiatied $LiVPO4F_{1-\delta}O_{\delta}$ synthesized via (a) CTR and (b) PTFE process (XRD peaks of Al foil of electrodes are shown at 38°, 44°, 64°, and 77° and inset is $VPO4F_{1-\delta}O_{\delta}$ structure obtained by Rietveld refinement (converted to a triclinic lattice as described in text)), and (c) comparison of average dihedral angles of VO_4F_2 octahedrons (Points and dashed lines represent experimental and calculation results, respectively.)

as in CTR process.[32, 33] Considering the relative molar volumes and experimental fluorine-rich or -poor synthesis conditions at high temperature, we can assume that DFT studies on $LiVPO_4F$ and $LiVPO_4F_{0.917}O_{0.083}$ can represent experimental PTFE and CTR sample, respectively.

Comparing to the PTFE process, possibility of the flourine loss during CTR process could be higher than the PTFE process. It is known that decomposition of $LiVPO_4F$ ($3LiVPO_4F \rightarrow Li_3V_2(PO_4)_3 + VF_3$ (gas)) can easily occur during the CTR process.[24] Also, the quenching step under air in the CTR process can be susceptible to oxidize the final product, and the degree of oxidation is not controllable in the CTR process. However, the PTFE process is proceeded under fluorine-rich environment due to excess amount of the fluorine caused by decomposition of the PTFE at synthesis temperature without any sequential quenching process, and thereby high purity of $LiVPO_4F$ in the sample is obtained.[14] The different fluorine environment of the two synthesis processes can induce different amount of the oxygen defect concentration in $LiVPO_4F$. Even though the PTFE process can make fluorine-rich environment during the synthesis, the $LiVPO_4F$ sample synthesized by the PTFE process has almost the ideal composition with the oxidation of V^{3+} indicating that it has negligible oxygen defects.[14] With all, we assume that DFT studies on $LiVPO_4F$ and $LiVPO_4F_{0.917}O_{0.083}$ can represent experimental PTFE and CTR sample, respectively.

3.3.2 Different phase transition (triclinic ↔ monoclinic) behavior of the delithiated phases ($VPO_4F_{1-\delta}O_{\delta}$) in the samples with different amount of O_F^-

To understand the possible formation of metastable triclinic phase in the delithiated phases ($VPO_4F_{1-\delta}O_{\delta}$, $\delta \geq 0$) depending on the amount of O_F^-, the two samples obtained from the PTFE and CTR process, which can have different amount of the oxygen defects, were electrochemically delithiated. Figure 7 shows the XRD patterns of $VPO_4F_{1-\delta}O_{\delta}$ electrodes of the CTR- and PTFE-synthesized $LiVPO_4F_{1-\delta}O_{\delta}$. Details of the XRD refinement are included in Supplementary Information (Table S3 and S4). Overall, the two samples have similar XRD patterns. However, slight difference in the local structure of the samples, especially the tilting angle of VO_4F_2 octahedra, is observed. Average dihedral angles of VO_4F_2 octahedra in the PTFE and

Table 3. Comparison of lattice parameters of $LiVPO_4F$ obtained by CTR process performed in the previous studies

	a (Å)	*b* (Å)	*c* (Å)	alpha (°)	beta (°)	gamma (°)	V/Z (Å^3)
CTR, ref[4]	5.170	5.308	7.263	107.59	107.97	98.39	87.18
CTR, ref[15]	5.175	5.314	7.301	108.95	107.21	98.38	87.39

CTR VPO_4F samples were calculated based on an average value of θ1 and θ2 shown in Figure 4. The average dihedral angle of VO_4F_2 octahedra in the CTR sample, which has higher concentration of O_F^- than the PTFE sample, is ~2.2°. It is comparable to the value in previous study (~1.6°),[23] whereas the average dihedral angle (~ 4.0°) of VO_4F_2 octahedra in the PTFE sample is larger than that the CTR process (~2.2°). Given that the DFT calculations in Figure 4 show that the dihedral angle can be used as an indicator to identify the degree of phase transition and the presence of O_F^-, the lower dihedral angle in the CTR sample than the PTFE sample indicates that the PTFE sample has smaller oxygen defect concentration than the CTR samples. Furthermore, the dihedral angle in the PTFE sample is still much higher than that in defect-free monoclinic VPO_4F optimized in DFT. Considering that the triclinic $VPO_4F_{1-\delta}O_\delta$ ($\delta \geq 0$) phase has higher average dihedral angle (16.61° and 15.20° for δ = 0 and 0.083, respectively) than the monoclinic one (2.65° and 2.46° for δ = 0 and 0.083, respectively) (Figures 3 and 4), the larger dihedral angle in the electrochemically delithiated PTFE sample can be possibly originated from mixtures of stable monoclinic and metastable triclinic $VPO_4F_{1-\delta}O_\delta$ phases or incomplete phase transformation from the triclinic to the monoclinic phase. In other words, it indicates that the phase transition from triclinic to monoclinic $VPO_4F_{1-\delta}O_\delta$ is almost completed in the CTR samples, not in the PTFE sample during delithiation process (= charge). From these results, we conclude that 1) the CTR-sample has higher concentration of O_F^- defect than the PTFE sample; 2) in both samples, triclinic $VPO_4F_{1-\delta}O_\delta$ phases are formed at first and then transformed to monoclinic; and 3) such phase transformation from the triclinic to monoclinic $VPO_4F_{1-\delta}O_\delta$ is incomplete in the PTFE sample, all of which can cause the change of redox reaction pathways in the $LiVPO_4F_{1-\delta}O_\delta$.

3.3.3 Change in the charge/discharge process of the samples by incorporation of O_F^-

Taking into account lattice parameters of $LiVPO_4F$ synthesized by the CTR process in the previous studies (Table 3), those of Piao *et al.*'s sample[15] were larger than that of Mba *et al.*'s,[4] and even close to that of the PTFE sample in this study. The molar volume of Piao *et al.*'s (V/Z=87.39 Å^3) sample was 0.24 % bigger than Mba *et al.*'s (V/Z=87.18 Å^3). It implies that Piao *et al.*'s sample might have a lower level of O_F^- than Mba *et al.*'s. Considering that the amount of the oxygen defects is not controllable in the CTR process, different molar volumes of the reported CTR samples can indicate different amount of oxygen defects. As a consequence, the discrepancy of redox reaction pathways in reported the samples synthesized by CTR process can be understood by the correlation of different amount of O_F^- with the symmetry of redox process investigated by the DFT calculation.

4. Discussion

In previous studies, both asymmetric and symmetric redox pathways of $LiVPO_4F$ were suggested (Figure 1) even though all of the samples were obtained by CTR synthesis process.[4, 15] We focused on understanding the effects of O_F^- on the stability of the delithiated phases, their phase transition behaviour, and the stability of the intermediate phases. Our experiments confirmed that the synthesis process can affect the amount of oxygen defects (Figure 6 and Table 2) and the structure of the fully delithiated VPO_4F phases (Figure 7). The discrepancy in the redox pathways of $LiVPO_4F$ reported in literature can be explained by integrating the experimental and computational results of $LiVPO_4F$ (~PTFE) and $LiVPO_4F_{1-\delta}O_\delta$ (~CTR) samples.

Figure 8 shows proposed redox reaction pathways based on our DFT calculations considering following assumptions. First, the charge and discharge processes are sequential processes of the delithiation/lithiation and phase transition between triclinic and monoclinic VPO_4F (and $VPO_4F_{1-\delta}O_\delta$) and vice versa. Second, only $Li_{0.667}VPO_4F$ (and $Li_{0.667}VPO_4F_{1-\delta}O_\delta$) is shown as a representative intermediate phase since this intermediate phase is most frequently reported from previous experiments.[4] Note that the proposed reaction pathways can be applicable to the other intermediate phases considering the comparable formation energies of other intermediate phases to $Li_{0.667}VPO_4F$ (and $Li_{0.667}VPO_4F_{1-\delta}O_\delta$). Third, metastable 'triclinic' VPO_4F (and $VPO_4F_{1-\delta}O_\delta$) can be an end-member in the charge process, since it retains the original symmetry of the lithiated $LiVPO_4F$ (and $LiVPO_4F_{1-\delta}O_\delta$) phase, and then this metastable triclinic phase undergoes the phase transition to stable monoclinic VPO_4F ($VPO_4F_{1-\delta}O_\delta$) by overcoming an activation barrier (Figures 3 and 7). Under these assumptions, during charging, the intermediate phase $Li_{0.667}VPO_4F$ (and $Li_{0.667}VPO_4F_{1-\delta}O_\delta$) is formed following the non-equilibrium path connecting $LiVPO_4F_{1-\delta}O_\delta$ and triclinic $VPO_4F_{1-\delta}O_\delta$ (path "1" in

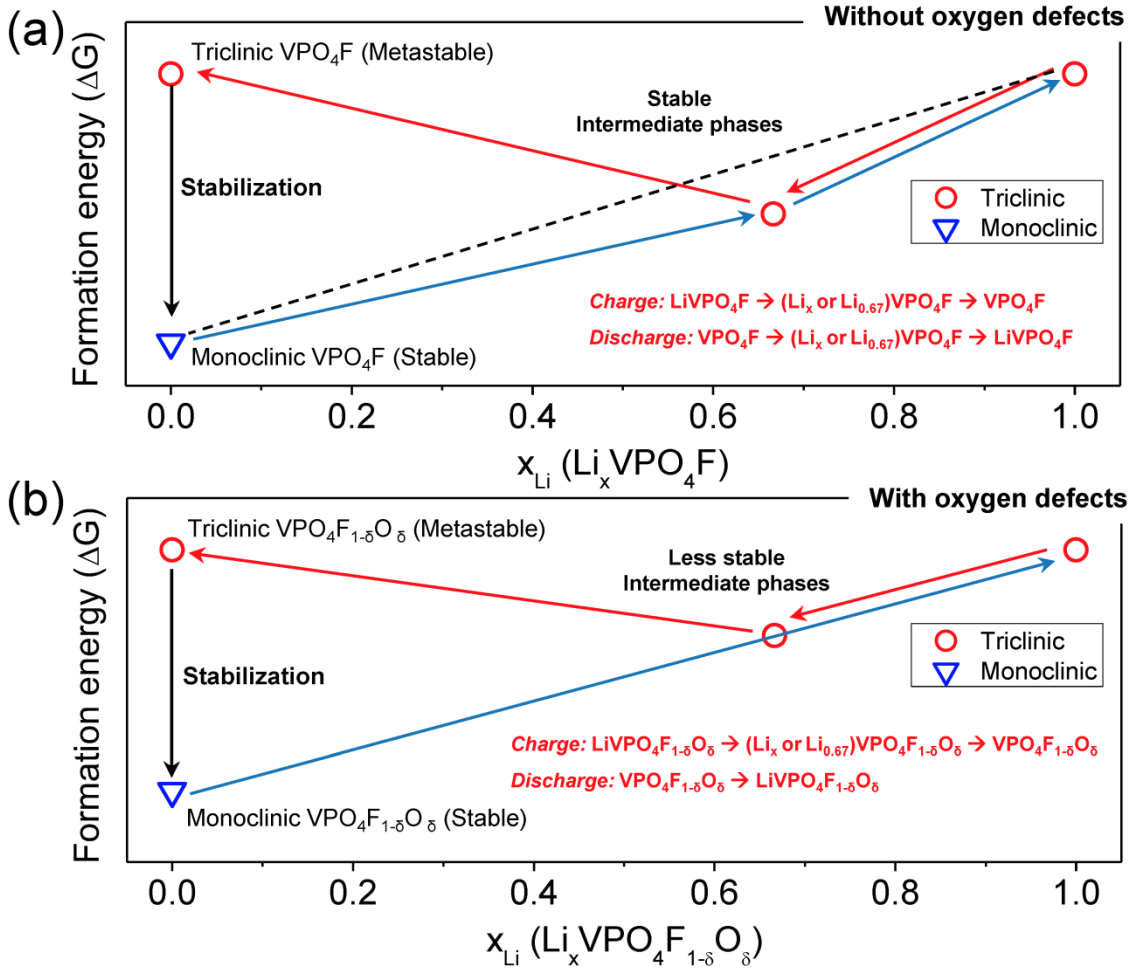

Figure 6. Schematic diagram of redox reaction pathways of (a) $LiVPO_4F$ (similar to the PTFE sample) and (b) $LiVPO_4F_{1-\delta}O_\delta$ (similar to the CTR sample) depending on stability of the delithiated VPO_4F and $VPO_4F_{1-\delta}O_\delta$ phases (red arrow: charge process, blue arrow: discharge process)

Figure 5) at first in both defect-free (~PTFE) and defective (~CTR) samples.

After that, redox reaction pathways can be differed by the presence of O_F^-. Several more intermediates are still accessible even after $VPO_4F_{1-\delta}O_\delta$ phase transformation from metastable triclinic to stable monoclinic phase (path "2" in Figure 5) for defect-free $LiVPO_4F$ system. Moreover, the average dihedral angles in the PTFE and CTR samples in Figure 7 indicate that the metastable triclinic $VPO_4F_{1-\delta}O_\delta$ is not fully transformed to stable monoclinic phase in the defect-free $LiVPO_4F$ sample, which increases the chance of formation of intermediate phases. Therefore, $Li_{0.667}VPO_4F$ can be formed during discharging as well as charging, leading to a symmetric redox pathway in the defect-free $LiVPO_4F$ such as the PTFE sample in this study and Piao *et al.*'s CTR sample.[15] On the contrary, the more oxygen defective CTR sample is more likely to complete the triclinic-to-monoclinic phase transformation of $VPO_4F_{1-\delta}O_\delta$, lowering the chance of formation of intermediate phases. For example, if the energy penalty for the nucleation and growth of the 2nd phase is not negligible, the formation of $Li_{0.667}VPO_4F_{.917}O_{0.083}$ whose Gibbs formation energy is 0.0 eV can be suppressed leading to an asymmetric redox pathway in the oxygen defective samples such as the CTR sample in this study and Mba *et al*'s CTR sample.[4]

If the electrochemical reactions of $LiVPO_4F$ follows the symmetric redox mechanism forming intermediate phases during both charge and discharge, its rate capability would be improved by reducing lattice mismatch between charged and discharged phases, especially in the material which has large lattice mismatch between two end-members. Interestingly, we observed that $LiVPO_4F$ produced by the PTFE process, which can have less amount of the oxygen defects and thereby can likely have the intermediate phases, exhibited greatly improved electrochemical performances compared to that of the CTR sample.[14] Optimization of the electrochemical performance of $LiVPO_4F$ can be shed light considering that the O_F^- can significantly affect the symmetry of reaction pathways in this system and its concentration is influenced by the materials synthesis methods.

Conclusions

The stability of the intermediate phases and the delithiated phases in $LiVPO_4F$ with respect to the presence of oxygen defects (O_F^-) and their influence on the symmetry of redox reaction were investigated via combined experimental-theoretical studies. First, we examined the stability of stable (monoclinic) and metastable (triclinic) VPO_4F with and without

the oxygen defects and combined this with the calculated total energies of the intermediate phases (Li_xVPO_4F and $Li_xVPO_4F_{1-\delta}O_\delta$, $0 < x < 1$). Our calculational results show that 1) the phase transition from metastable triclinic to stable monoclinic $VPO_4F_{1-\delta}O_\delta$ phase is almost spontaneous with < 5 meV/f.u. energy barrier in both defect-free and defective systems; 2) along the non-equilibrium pathway between triclinic $LiVPO_4F_{1-\delta}O_\delta$ and triclinic $VPO_4F_{1-\delta}O_\delta$, both defect-free and defective systems likely form several intermediates; and 3) along the equilibrium pathway between triclinic $LiVPO_4F_{1-\delta}O_\delta$ and monoclinic $VPO_4F_{1-\delta}O_\delta$, the formation of most intermediates is unlikely in defective $LiVPO_4F_{0.917}O_{0.083}$ system, while several intermediates are still energetically favourable in the defect-free $LiVPO_4F$ system. Second, our experiments inform that 1) the PTFE and CTR synthesis processes provide different fluorine environments, resulting in different amount of O_F^- defect; 2) in the PTFE sample where the O_F^- concentration is lower than the CTR sample, the metastable triclinic VPO_4F was not fully relaxed to stable monoclinic variant at the end of charging. Combining our results in calculations with experiments, we conclude that the asymmetric redox reaction pathway could be originated from the formation/stabilization of metastable $VPO_4F_{1-\delta}O_\delta$ phases and low stability of the intermediate phase ($Li_{0.667}VPO_4F_{1-\delta}O_\delta$) caused by O_F^-. On the other hand, reducing the amount of O_F^- can lead to formation of the intermediate phases during both discharging and charging, resulting in a symmetric redox reaction pathway. This study implies that the formation of intermediate phases during discharging can depend on experimental conditions such as synthesis processes that can affect the amount of O_F^-. This finding will contribute further optimization of the electrochemical performance of tavorite $LiVPO_4F$ cathode materials.

Conflicts of interest

There are no conflicts to declare.

Acknowledgements

This work was supported by the National Institute of Supercomputing and Network/Korea Institute of Science and Technology Information with supercomputing resources including technical support (KSC-2016-S1-0038). Part of the work was performed under the auspices of DOE by Lawrence Livermore National Laboratory under Contract DE-AC52-07NA27344.

References

1 J. M. Tarascon and M. Armand, *Nature*, 2001, **414**, 359.
2 A. Kraytsberg and Y. Ein-Eli, *Advanced Energy Materials*, 2012, **2**, 922-939.
3 J. W. Fergus, *Journal of Power Sources*, 2010, **195**, 939-954.
4 J.-M. A. Mba, L. Croguennec, N. I. Basir, J. Barker and C. Masquelier, *Journal of The Electrochemical Society*, 2012, **159**, A1171-A1175.
5 M. Ati, M. T. Sougrati, G. Rousse, N. Recham, M. L. Doublet, J. C. Jumas and J. M. Tarascon, *Chemistry of Materials*, 2012, **24**, 1472-1485.
6 A. Sobkowiak, M. R. Roberts, L. Häggström, T. Ericsson, A. M. Andersson, K. Edström, T. Gustafsson and F. Björefors, *Chemistry of Materials*, 2014, **26**, 4620-4628.
7 R. Malik, A. Abdellahi and G. Ceder, *Journal of The Electrochemical Society*, 2013, **160**, A3179-A3197.
8 R. Malik, F. Zhou and G. Ceder, *Nature Materials*, 2011, **10**, 587.
9 H. Liu, F. C. Strobridge, O. J. Borkiewicz, K. M. Wiaderek, K. W. Chapman, P. J. Chupas and C. P. Grey, *Science*, 2014, **344**.
10 C. Delmas, M. Maccario, L. Croguennec, F. Le Cras and F. Weill, *Nature Materials*, 2008, **7**, 665.
11 Y. Orikasa, T. Maeda, Y. Koyama, H. Murayama, K. Fukuda, H. Tanida, H. Arai, E. Matsubara, Y. Uchimoto and Z. Ogumi, *Journal of the American Chemical Society*, 2013, **135**, 5497-5500.
12 S.-i. Nishimura, R. Natsui and A. Yamada, *Angewandte Chemie International Edition*, 2015, **54**, 8939-8942.
13 M. Kim, S. Lee and B. Kang, *Chemistry of Materials*, 2017, **29**, 4690-4699.
14 M. Kim, S. Lee and B. Kang, *Advanced Science*, 2016, **3**, 1500366-n/a.
15 Y. Piao, Y. Qin, Y. Ren, S. M. Heald, C. Sun, D. Zhou, B. J. Polzin, S. E. Trask, K. Amine, Y. Wei, G. Chen, I. Bloom and Z. Chen, *Physical Chemistry Chemical Physics*, 2014, **16**, 3254-3260.
16 T. Bamine, E. Boivin, F. Boucher, R. J. Messinger, E. Salager, M. Deschamps, C. Masquelier, L. Croguennec, M. Ménétrier and D. Carlier, *The Journal of Physical Chemistry C*, 2017, **121**, 3219-3227.
17 G. Kresse and J. Furthmüller, *Physical Review B*, 1996, **54**, 11169-11186.
18 P. E. Blöchl, *Physical Review B*, 1994, **50**, 17953-17979.
19 J. P. Perdew, M. Ernzerhof and K. Burke, *The Journal of Chemical Physics*, 1996, **105**, 9982-9985.
20 I. A. Vladimir, F. Aryasetiawan and A. I. Lichtenstein, *Journal of Physics: Condensed Matter*, 1997, **9**, 767.
21 L. Wang, T. Maxisch and G. Ceder, *Physical Review B*, 2006, **73**, 195107.
22 T. Mueller, G. Hautier, A. Jain and G. Ceder, *Chemistry of Materials*, 2011, **23**, 3854-3862.
23 B. L. Ellis, T. N. Ramesh, L. J. M. Davis, G. R. Goward and L. F. Nazar, *Chemistry of Materials*, 2011, **23**, 5138-5148.
24 J.-M. Ateba Mba, C. Masquelier, E. Suard and L. Croguennec, *Chemistry of Materials*, 2012, **24**, 1223-1234.
25 G. Henkelman, B. P. Uberuaga and H. Jónsson, *The Journal of Chemical Physics*, 2000, **113**, 9901-9904.
26 G. Mills, H. Jónsson and G. K. Schenter, *Surface Science*, 1995, **324**, 305-337.
27 H. JÓNSSON, G. MILLS and K. W. JACOBSEN, in *Classical and Quantum Dynamics in Condensed Phase Simulations*, WORLD SCIENTIFIC, 2011, DOI: 10.1142/9789812839664_0016, pp. 385-404.
28 D. Sheppard, P. Xiao, W. Chemelewski, D. D. Johnson and G. Henkelman, *The Journal of Chemical Physics*, 2012, **136**, 074103.
29 P. Xiao and G. Henkelman, *The Journal of Chemical Physics*, 2012, **137**, 101101.
30 P. Xiao, J.-G. Cheng, J.-S. Zhou, J. B. Goodenough and G. Henkelman, *Physical Review B*, 2013, **88**, 144102.
31 P. Haas, F. Tran and P. Blaha, *Physical Review B*, 2009, **79**, 085104.

32 M. D. Radin and D. J. Siegel, *Energy & Environmental Science*, 2013, **6**, 2370-2379.
33 H. Shiiba, N. Zettsu, M. Nakayama, S. Oishi and K. Teshima, *The Journal of Physical Chemistry C*, 2015, **119**, 9117-9124.

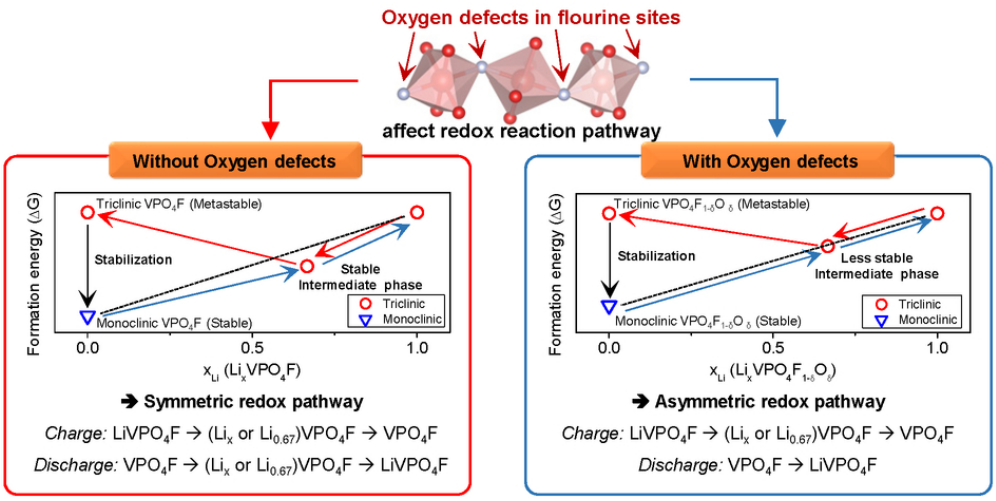

80x39mm (300 x 300 DPI)